Diamond graphitization by laser-writing for all-carbon detector applications

M. De Feudis [a,b,*], A.P. Caricato [a,b], A. Taurino [c], P.M. Ossi [d], C. Castiglioni [e], L. Brambilla [e], G. Maruccio [f], A.G. Monteduro [f], E. Broitman [g], G. Chiodini [b], M. Martino [a,b]

[a] Department of Mathematic and Physics, University of Salento, 73100 Lecce, Italy
[b] INFN National Institute of Nuclear Physics, 73100 Lecce, Italy
[c] CNR-IMM Institute for Microelectronics and Microsystem, 73100 Lecce, Italy
[d] Dipartimento di Energia, Politecnico di Milano, 20133 Milan, Italy
[e] Dipartimento di Chimica, Materiali, Ingegneria Chimica, Politecnico di Milano, 20133 Milan, Italy
[f] NNL-CNR Nanotec, 73100 Lecce, Italy
[g] IFM, Linköping University, SE58183 Linköping, Sweden

The surface of a detector grade CVD polycrystalline diamond sample (5 × 5 × 0.05 mm^3) was irradiated by an ArF excimer laser (λ = 193 nm, τ = 20 ns) to produce graphitic conductive layers.
In particular, two sets of four parallel graphitic strip-like contacts, with 1 mm pitch, were created along the whole sample on the top and on the rear surfaces of the sample respectively. The two series of stripes lie normally to each other. Such a grid allows to obtain a segmented all-carbon device capable of giving bi-dimensional informa-tion on particle detection processes in nuclear applications.
Afterwards, an extensive characterization of the samples was performed: SEM and micro-Raman investigations to study the morphological and structural evolution of the irradiated areas, EDS measurements to individuate any absorption phenomena from environment associated to laser treatment, and nanoindentation mapping to un-derstand how the hard-soft transformation occurred depending on the locally transferred energy. Finally, cur-rent-voltage analyses were carried out checking the ohmic behavior of the diamond-graphite contact. By comparing the results of the different characterization analyses, a strong periodicity of the modified surface prop-erties was found, confirming the reliability and reproducibility of the laser-induced graphitization process. The results demonstrate that the laser-writing technique is a good and fast solution to produce graphitic contacts on diamond surface and therefore represents a promising way to fabricate segmented all-carbon devices.

Keywords:
Diamond film
Graphitization
Surface characterization
Ohmic contacts
All-carbon detectors

1. Introduction

The physical properties of diamond, such as the radiation hardness, high thermal conductivity, large bandgap, high carrier mobility, chemical stability, bio-inertness and biological tissue equivalence, have proved to be attractive for different applications. In particular, diamond devices are considered performing sensors for detection, beam monitoring and time of flight measurements in nuclear physics [1–3], and besides dosimetry in medical applications [4,5]. In order to exploit the great potentialities of diamond sensors, a significant effort for electrical contacting is required. In particular, good adhesion, stability, radiation hardness and ohmic behavior are required properties for electrodes on diamond surfaces.

Traditionally, electric contacts on diamond are produced by metal layer deposition. This technique involves many complex process steps, such as surface cleaning, carbide formation with Cr or Ti, thermal annealing, metal contact layer deposition with Au or W, and lithography process for strip or pixel patterning [6]. Metalized contacting of diamond devices, notwithstanding such a time consuming and expensive treatment, often present adhesion issues, poor stability and radiation hardness, besides a non-ohmic behavior. This work aims at demonstrating that it is possible to create ohmic contacts on diamond surfaces by an alternative technique of laser-writing, involving a single process step, performed in air, at standard ambient conditions.

During the last decades, several studies on diamond graphitization by laser-writing have been carried out [7–16]. The key idea at the basis of the process is to take advantage about the existence of different carbon allotropes. Indeed, this technique allows inducing a local diamond-graphite transformation led by the fact that the graphite is the thermodynamically stable carbon phase at room pressure and

* Corresponding author at: Department of Mathematics and Physics, University of Salento, 73100 Lecce, Italy.
E-mail address: mary.defeudis@le.infn.it (M. De Feudis).

Article history:
Received 30 October 2016
Received in revised form 21 December 2016
Accepted 21 December 2016
Available online 26 December 2016

Published Journal Article available at: http://dx.doi.org/10.1016/j.diamond.2016.12.019

temperature [17]. In our previous works, several studies on diamond graphitization were carried out to better understand the laser-induced process and its potentiality. In particular, an extensive work of optimization of the laser irradiation parameters to produce homogeneous, low resistivity graphitic strip-like contacts on diamond surface was performed (resistivity values of the order of 10^{-5} Ωm were obtained) [18]. Then, a first all-carbon detector was produced and characterized by nuclear investigations. First, a comparison between the performances of an all-carbon device and those of a metallized diamond was carried out with a 500 MeV electron beam at the Beam Test Facility (BTF), Frascati (Italy), demonstrating similar characteristics of the two detectors [19]. A more complex investigation was later performed with a 120 GeV pion beam at CERN infrastructures showing good nuclear detection performances of all-carbon device, with a charge collection efficiency (CCE) of 42% (in agreement with expected value reported on supplier datasheet) [18].

Based on these studies, a new work carried out in the framework of the PADME project (Positron Annihilation into Dark Matter Experiment) and supported by the Italian National Institute of Nuclear Physics (INFN) [20], is presented in this paper. In particular, the PADME experiment aims to study the interaction between positrons and electrons during annihilation processes in a diamond active target looking for a potential dark photon. Some extensions of the Standard Model suggest that when a positron-electron annihilation happens, one of the two generated gammas could mix in an invisible dark photon [21]. The diamond detector designed for this project is a segmented all-carbon device, with graphitic electrodes. The choice of graphitized diamond (rather than a metallized device) working as target is crucial as PADME project aims to minimize the bremsstrahlung cross-section. Indeed, the bremsstrahlung cross-section due to a positron-electron interaction scales as the atomic number square Z^2 of the target, with respect to the annihilation cross-section which scales as the atomic number Z of the target [22]. In this way, the minimization of the degradation of the positron beam in terms of energy and trajectory is obtained by the use of diamond.

Usually, diamond graphitization process have been developed for small detector areas (few squared millimetres), which means manufacturing graphitized electrodes of only few hundreds of micrometres wide. On the contrary, for PADME project, an all-carbon target with large dimensions ($20 \times 20 \times 0.05$ mm^3) is required with electrodes having a width closed to 1 mm, which means producing of very large contacts.

In this paper, the production of large graphitic electrodes covering both diamond surfaces by laser-writing was studied and carried out. A wide work of characterization was performed by Scanning Electron Microscopy, micro-Raman Spectroscopy, Energy Dispersion X-ray Spectroscopy, Hardness and Elastic Modulus mappings, and current-voltage measurements to gain better insight into the diamond-graphite laser induced transformation of a large area and to verify the ohmic nature of the contact. The feasibility, homogeneity and reproducibility of the large-area diamond graphitization were also verified.

2. Material and methods

2.1. Manufacturing of graphitic contacts on diamond surface by laser-writing

A very simple experimental apparatus was developed to produce graphitic layers on diamond surface. In particular, in order to produce bi-dimensional conductive structures we used a set-up based on an excimer laser ($\lambda = 193$ nm, $\tau = 20$ ns, $\nu = 10$ Hz), an objective focusing lens and two motorized stages, working in air, under LabVIEW control and in a short irradiation time. In order to produce so large graphite electrode it was necessary to rearrange and test the laser-induced graphitization process developed previously for small detectors with thin electrodes [18].

The starting sample characterized in this paper was a detector grade CVD (chemical vapor deposition) polycrystalline diamond provided by Applied Diamond Inc. (USA) with a dimension of only $5 \times 5 \times 0.05$ mm^3 in order to limit sample costs [23]. The diamond had a low impurity content (nitrogen concentration < 1 ppb), a roughness <5 nm Ra for the polished surface (nucleation side) and <1.5 μm Ra for the unpolished surface (growth side), and an electric resistivity >10^{12} Ωm.

In order to create a segmented all-carbon detector, four large graphitic strips covering almost the whole diamond surface area were produced on both sides. The laser worked with a fixed fluence equal to 5 J/cm^2, with a energy per pulse of 0.9 mJ and a laser power density of 0.25 GW/cm^2, producing a spot diameter size of 150 μm.

In Fig. 1(a), a picture of the sample after the laser treatment, obtained by an optical microscope, is reported: four strips vertically oriented on the top side are visible. The strip dimensions are 4×0.85 mm^2, with a pitch of 1 mm and a gap between two consecutive strips of 0.15 mm. In Fig. 1(b), a defocused picture of the graphitized diamond is shown in order to visualize both, the 4 vertical strips (top surface) and the 4 horizontal strips (bottom surface), indicated with 1, 2, 3, 4 and 5, 6, 7, 8, respectively. This electrode configuration is crucial to obtain bi-dimensional information during the detection process.

To satisfy all the electrode geometric characteristics required by the nuclear detection experiment (contact dimensions, fixed pitch at 1 mm and a small dead gap between two consecutive electrodes) [20], it was

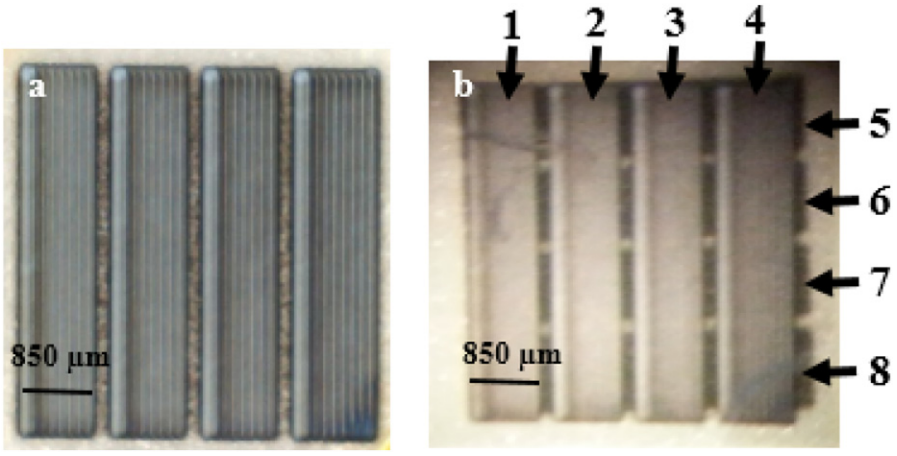

Fig. 1. Focused (a) and unfocused (b) optical microscope images of the segmented all-carbon sensor. Four graphitic contacts with vertical orientation (named 1, 2, 3, 4) and four horizontal contacts (indicated as 5, 6, 7, 8), are visible. Strip dimensions: 4×0.85 mm^2; pitch of 1 mm and inter-strip dead gap of 0.15 mm.

necessary to arrange the manufacturing of every large strip-like contact as the sum of several smaller strips (scans) partially overlapped each other. Indeed, taking into account that the laser system has a spot size diameter of 150 μm wide, different consecutive small scans were necessary to reach a width slightly lower than 1 mm. In addition, an overlap between two consecutive strips was planned in order to avoid the presence of unirradiated zone (harmful to the proper functioning of the electrical contact). Therefore, during the manufacturing of every single graphitic contact, a fixed laser horizontal shift of 100 μm was adopted for the production of two consecutive small strips, providing an overlapping configuration for both sides of every small strip. As a result, a strong periodicity in morphological and structural changes results within every graphitic electrode. Eight small vertical strips were necessary to get one large graphitic contact of 850 μm wide, and four graphitic large strips were created for every sample side to cover all diamond surfaces.

It is worth noting that this particular configuration of electrodes, which are orthogonally oriented in the two sides, is crucial for obtaining bi-dimensional information during the detection processes. This is a peculiar feature for an all carbon detector of this large scale.

2.2. Characterization techniques

An extensive work aimed at the morphological, compositional, structural, mechanical and electrical characterization of the sensors was carried out. In particular, Scanning Electron Microscopy (SEM) and Energy Dispersive X-ray Spectroscopy (EDS) analyses were performed by using a dual beam NVISION 40 Focused Ion Beam instrument, equipped with a high-resolution SEM GEMINI column. The instrument is also equipped with an INCA 350 X-Act detector allowing compositional analyses by energy dispersive X-ray spectroscopy. Micro-Raman Spectroscopy analysis was performed by using a Jobin Yvon Labram HR800 Raman spectrometer equipped with an Olympus BX41 microscope and an X–Y computer controlled moving stage (1 μm of spatial resolution). The spectra were recorded using the 514.5 nm exciting line of an Ar^+ laser (20 mW). The laser beam was focused on the samples by a 50× objective. Every spectrum was obtained as the average of four acquisitions each lasting 20 s. Mechanical properties were studied by a Triboindenter TI950 (Hysitron) working with a Berkovich diamond probe at room temperature and 40% relative humidity. The penetration depth of the indenter on the treated surfaces was limited to 15 nm (<10% of the possible total thickness [18]) to avoid any effect from the substrates. The hardness (H) and reduced elastic modulus (Er) were calculated following the model of Oliver and Pharr using the unloading elastic part of the load-displacement curve [24]. Hardness and reduced elastic modulus maps were performed with multiple indents in $10 \times 120\ \mu m^2$ areas to analyze the variations of mechanical properties on the irradiated zones. Current-voltage measurements were carried out to verify the electrical properties of the produced graphite electrodes and the nature of the diamond-graphite contact. The investigations were performed using a probe station composed by two probes with tungsten tips of 40 μm in diameter moved by two micromanipulators, and a LabVIEW software to control a Yokogawa 7651 programmable DC source, a SR570 low noise current preamplifier and a HP34410 digital multimeter. In particular, the resistivity of the graphitic strips was evaluated by means of the transmission line model (TLM) [25].

3. Graphitic contact surface characterizations

3.1. Morphological investigations

Traditionally, a good technique to appreciate laser-induced morphological modifications on diamonds is the scanning electron microscopy [11,26,27]. The SEM image in Fig. 2 evidences the changes of the graphitized diamond surface at two different magnification scales. In particular, the inset in the top-right corner shows the sub-structure of one of the large strip in Fig. 1(a). Every single large strip is composed of eight thinner strips each related to a single laser scan. The SEM image reveals a periodic contrast modulation, perpendicular to the strip length, which is clearly highlighted by the integrated contrast profile obtained from the area in the rectangle (the rectangle height corresponds to the integration width, whereas the rectangle base is the length of the contrast line scan, of about 225 μm). It is worth noting that this contrast modulation has a periodicity of about 100 μm, as expected considering the experimental conditions.

By analyzing the SEM image, it is also possible to identify the main contrast variations highlighted in the picture by white dashed lines: i) the presence of brighter (A) and darker (B) regions within each strip and ii) the presence of lens-shape dark details (C), running along every strip and about 10 μm wide. In this section, these contrast

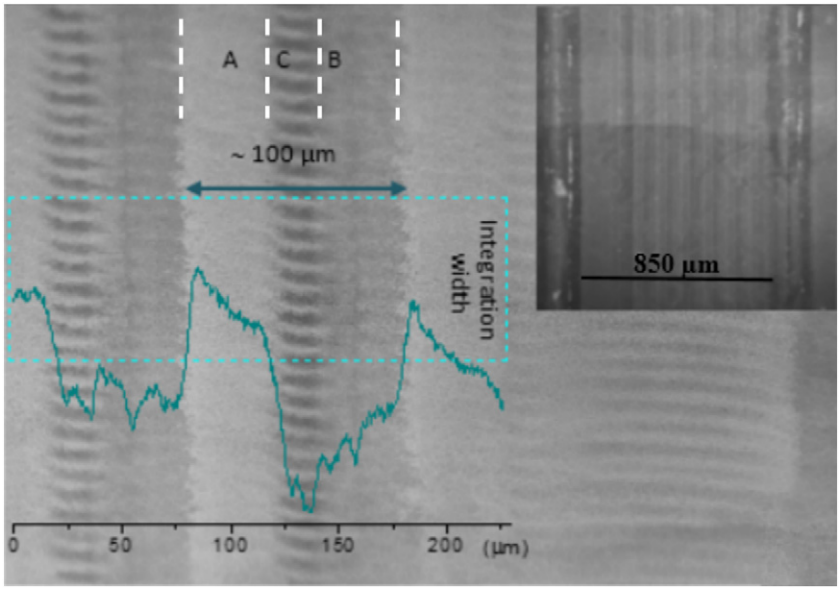

Fig. 2. SEM image of a laser-induced graphitic strip on the diamond surface and integrated contrast profile acquired from the dashed green rectangular area in the image. Three different regions, A, B and C can be identified on the basis of the optical contrast. An overview of the whole strip is shown in the top-right inset.

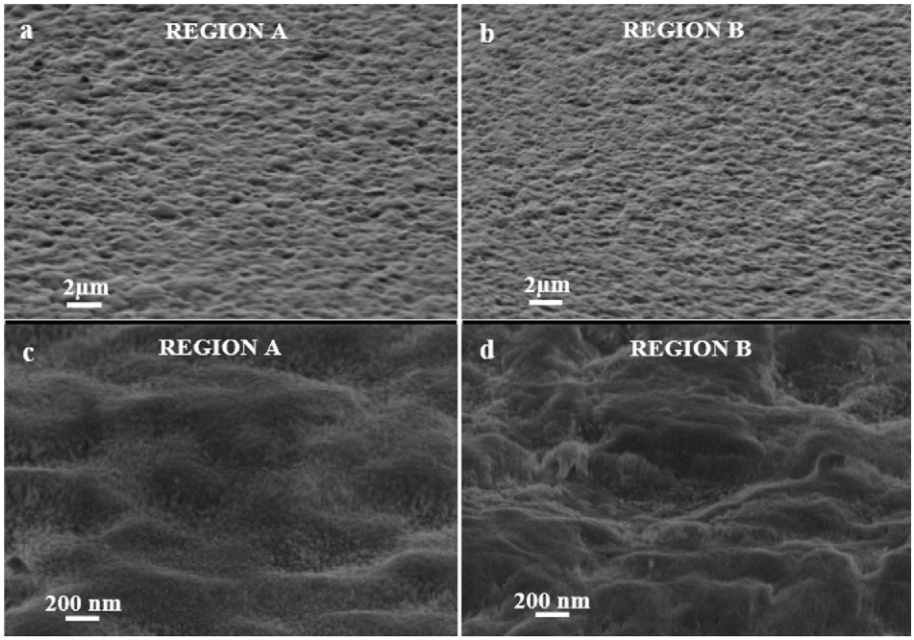

Fig. 3. Comparison of the surface topography of the regions A and B at low (a) and (b), and at high magnification (c) and (d), respectively.

variations are analyzed from a morphological point of view and correlated with the laser graphitization process.

Fig. 3(a) and (b) compare the surface morphology of the regions A and B respectively. The images were acquired with the sample tilted at 45° with respect to the incident electron beam in order to enhance the topographical features of the surface. The surface of region B exhibits a higher density of holes and swellings, suggesting an increase of the laser induced damage. This is confirmed by the high magnification images of the same regions reported in Fig. 3(c) and (d). The surface modification is here evident at the nanoscale, in particular the presence of small grains, resulting from material ablation/redisposition. Fig. 4 reports the high magnification image of the region C; in particular, the bottom part of the image reveals the enhanced surface damage of the lens-shaped darker region, in comparison with the surrounding smoother areas. These morphological differences inside every laser scan and periodically distributed along every large strip (contact) are related to the laser beam energy distribution inside the laser spot and to the overlapping phenomena. In particular, the higher damage induced in region C is due to the higher energy density in the center of the laser spots. The peculiar lens-shaped regions are reminiscent of the beam footprints during the vertical displacements of the laser processing. On the contrary, regions A and B are related to the irradiation from the laser beam lateral tails. In particular, their modification is lower than in the zone C, due to less energy absorbed. Small differences detectable in A and B regions, could be ascribed to a small asymmetry of the energy distribution in the beam tails.

Fig. 5 shows the SEM image of the boundary between treated and untreated sample areas. A transition region, with a width of about 5 μm, is evident between the undamaged and the laser graphitized surface.

3.2. Compositional analysis

To individualize any modification of the material due to reactions with chemical species from the environment associated to laser treatment, EDS analyses were performed. In particular, the three regions, highlighted by the white boundary lines, showing the contrast features previously discussed, were analyzed. Fig. 6(a) and (b) show the investigated areas and the acquired spectra, respectively.

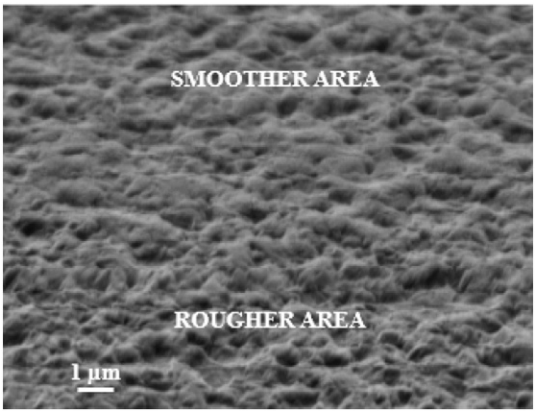

Fig. 4. Surface morphology of region C, showing topographic differences between the bottom part of the image (darker region of the C area shown in Fig. 2) and the top part of the image (brighter region of the C area shown in Fig. 2). The image suggests an enhanced roughness in the bottom region.

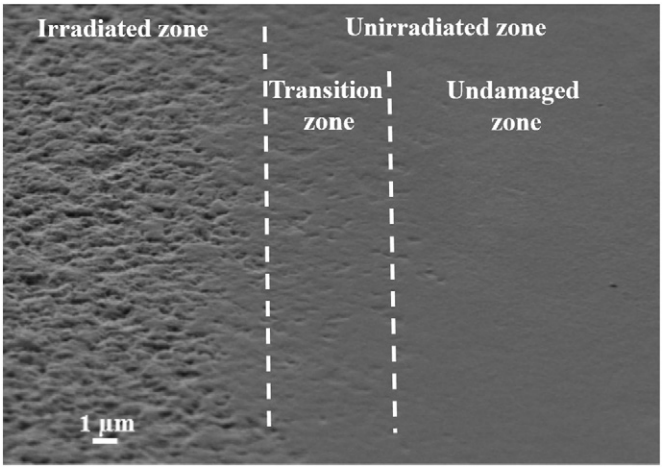

Fig. 5. Surface morphology of the boundary between treated and untreated regions.

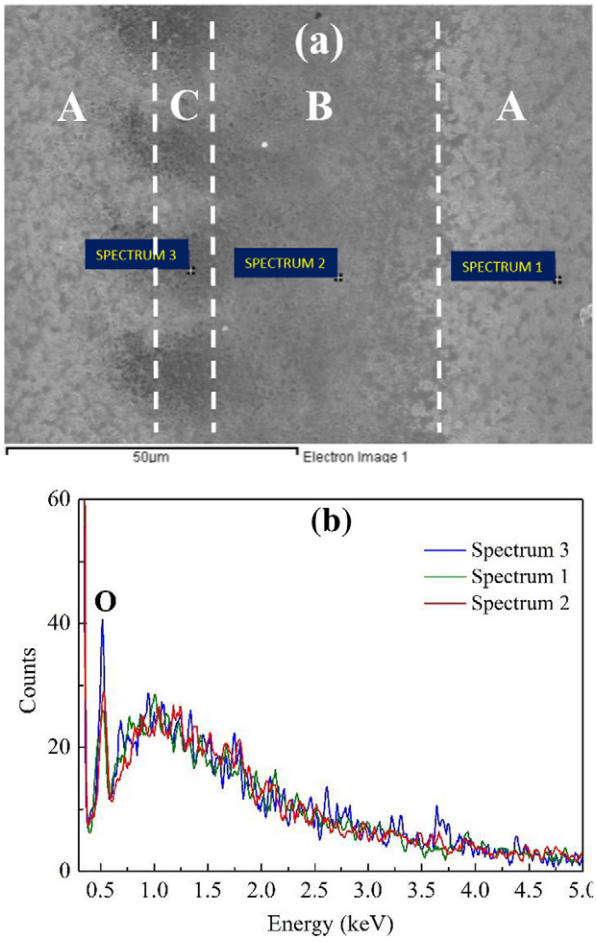

Fig. 6. (a) EDS analyses performed on three different contrast areas (A, B and C regions) and (b) the corresponding spectra.

In addition to the obvious presence of the carbon peak due to both diamond and graphite phases (not illustrated here), EDS spectra show the presence of an oxygen peak (O). The oxygen localized in the irradiated areas suggests a widespread absorption process from atmospheric air related to the great reactivity of the carbon atom dangling chemical bonds formed under laser treatment, enhanced by high temperature at the molten target surface; moreover, deep UV laser irradiation can promote dissociation of O_2 molecules. An increase of the oxygen signal was detected moving from regions A and B (spectra 1 and 2, respectively) to the region C (spectrum 3), (Fig. 6a). In particular, zones A and B show an oxygen peak of comparable intensity while a significant higher signal is appreciable in the zone C according to the increase deposited energy density. The trends described above were confirmed by repeating the EDS analysis in different points of the samples. Based on the above observations we propose that an enhanced oxidation process could be related to the higher surface damage observed in these regions of the sample.

3.3. Structural investigations

To describe the structural changes induced by the laser processing at the molecular level, a study by micro-Raman spectroscopy was carried out.

Several works appeared in the literature applying this technique for the characterization of ohmic contacts obtained by laser induced graphitization of diamond samples [10,12,14–16,26,28]. In these studies, the extent of the material modification was monitored considering the evolution of the intensity of the G band, at about 1580 cm^{-1} and arising from graphitic domains. Moreover, the appearance of a D band (at about 1350 cm^{-1}) allowed to extract information regarding the degree of disorder characterizing the sp^2 carbon phase obtained.

In the present work, the Raman technique was employed in order to obtain a qualitative estimation of the degree of graphitization/amorphization of the material belonging to the different areas identified by SEM measurements and by visual inspection of the optical microscope images.

Taking into account the periodicity of the laser-induced morphological modifications, we performed a Raman mapping recording spectra at different points along a line orthogonal to a strip. Twenty-one measurements with a step of 5 µm were performed with the aim of investigating the three regions showing the major contrast features. In particular, the mapping starts from the center of a C region, crosses A and B areas and ends in the subsequent C region (see Fig. 7).

In Fig. 8, several representative Raman spectra are reported, showing characteristic patterns, which can be ascribed to differently modified carbon. The Raman spectrum of the unirradiated material is also reported in Fig. 8. This spectrum was recorded in a region of the sample distant from strip-like contacts. It shows only the characteristic features of pure diamond, with the sharp Raman line at 1332 cm^{-1} confirming the good quality of the starting CVD polycrystalline diamond sample. Indeed, the spectrum does not show features which can be ascribed to the presence of disordered (e.g. amorphous) carbon, nor to the presence of graphitic domains.

Labels A, B, C in Fig. 8 indicate spectra obtained from different regions of a strip-like contact, showing different morphology. All these spectra clearly show features ascribed to graphitic material; moreover, the characteristic Raman line of diamond appears in all spectra, showing an intensity modulation associated to a change of the measurement point. The presence of two broad features (namely the G and D bands) can be taken as the signature of the presence of small-sized graphitic domains and/or of the presence of disordered graphitic material [29,30]. Indeed, the D band is silent in highly crystalline graphite or graphene, because of symmetry selection rules, and it rises in the presence of defects (chemical defects or structural imperfections) as well as when π electrons are confined into small graphene-like islands [31,32]. The presence of the line at 1332 cm^{-1} suggests that some diamond domains survive in the irradiated regions of the sample, may be because of

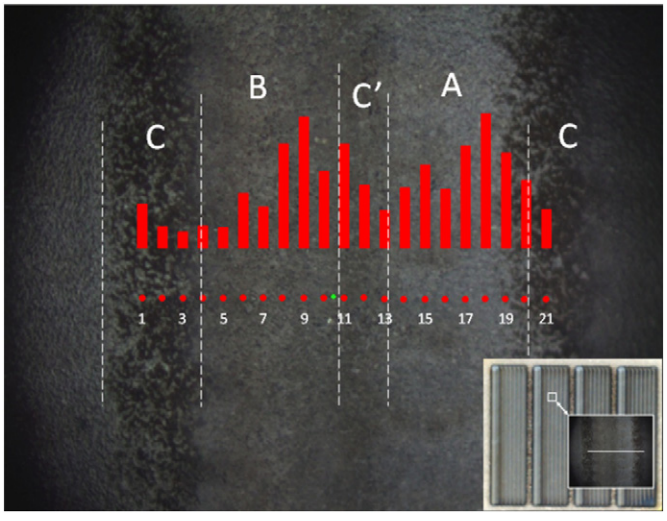

Fig. 7. Optical microscopy image of a selected area of a strip. A, B and C regions can be identified on the basis of the optical contrast. Notice the transition region labeled C′ between A and B regions (vertical white dotted lines are shown as guide for the eye). Red dots separated by 5 µm along the horizontal pathway indicate the points analyzed by Raman spectroscopy. The histogram describes the evolution of the integrated Raman intensity of the diamond Raman line (1332 cm^{-1}). An overview of the investigated zone is shown in the bottom-right corner.

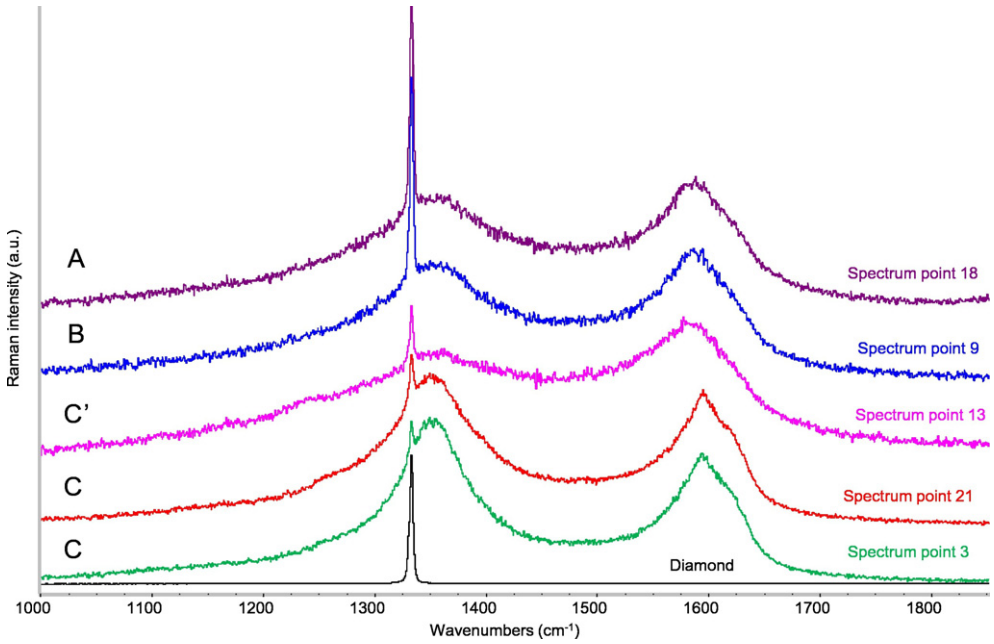

Fig. 8. Plot of Raman spectra representative of the different regions analyzed by Raman mapping (see Fig. 7 to identify the points of measurement). At the bottom, the Raman spectrum of the unirradiated diamond (black line) is reported for comparison.

inhomogeneity in the graphitization of the material (see Figs. 6 and 7). An alternative explanation could be given considering that the exciting laser beam is also probing the pristine diamond bulk extending below the graphitized/amorphized surface. However, due to the high absorption coefficient of graphite in the visible range, this behavior is expected only in presence of very thin graphitized domains, extending in depth only for few atomic layers [33].

A careful comparison among the spectra reported in Fig. 8 shows non-negligible differences in band shape and in the intensity pattern, which could be ascribed to the unavoidable inhomogeneity of the modified carbon material. Differently to the spectra recorded in the other regions, the two spectra representative of region C show a sharp G peak. Such a region is characterized by a more effective graphitization, in agreement with the morphological analysis. This finding suggests that in the region C more extended and regular graphitic islands are present.

It is possible to obtain a qualitative estimate and to map the degree of graphitization in the different points analyzed following the evolution of the Raman intensity of the diamond band, moving across the strip. This is illustrated by the histogram reported in Fig. 7, which shows a clear modulation of the diamond content, that is low in region C while increases remarkably in regions A and B. It is possible to notice the presence of a region previously not identified (labeled C′ in Fig. 7), located at the edge between A and B areas, and characterized by a relatively low diamond content. A possible explanation of this behavior is the partial overlapping of the irradiated regions during the laser fabrication of two adjacent thin strips: the enhanced graphitization of region C′ could result from the fact that it underwent double laser irradiations, both effective in promoting the carbon transformation from sp^3 to sp^2 carbon structure. Interestingly, according to the geometrical parameters adopted during the "writing" of the stripes, also regions A and B have been exposed twice to the photon beam, during two subsequent laser scans. The higher content of diamond observed in these regions can be justified as due to partial ablation of the graphitic material grown during the first scan, and subsequently damaged during the second scan. The balance between processes responsible of graphitization and laser induced carbon ablation is then crucial in determining the structure of the resulting modified material [7,18].

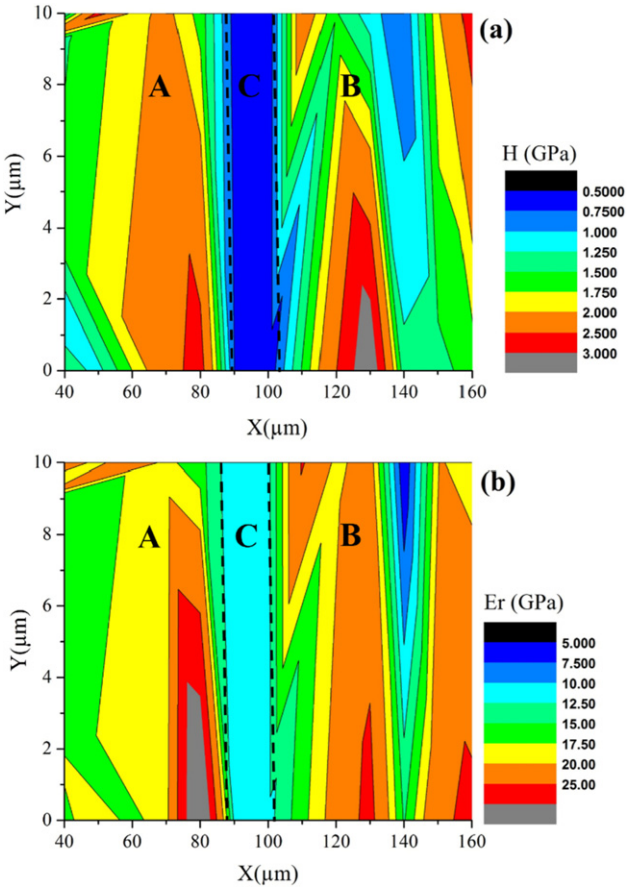

Fig. 9. Hardness (a) and reduced elastic modulus (b) mappings of a portion of a single laser-induced strip. A, B and C regions can be identified on the basis of the mechanical property contrast.

3.4. Nano-mechanical characterizations

Nano-indentation maps were performed to study the changes on the mechanical properties of the irradiated surface and to demonstrate the feasibility and the reliability of the laser-writing technique. Fig. 9(a) and (b) show hardness (H) and reduced elastic modulus (E_r) for three different regions, A, B and C, previously studied (Fig. 2).

Both maps clearly show the modified graphitic surface (vertical band-like) with lower hardness and lower elastic modulus with respect to the substrate. Indeed, for the unirradiated surface the hardness and elastic modulus average values are (2.35 ± 0.17) GPa and (23.2 ± 2.0) GPa, respectively. After the laser processing the H and E_r average values are (0.60 ± 0.05) GPa and (12.5 ± 1.0) GPa, respectively. The change in the mechanical properties can be correlated to the morphological changes. For example, in Fig. 9(a), it is possible to see a softer central region with two adjacent strip-like harder zones on the two sides (which are however less hard than the unirradiated surface). These three areas coincide with the three regions A, B, and C identified and characterized by SEM and Raman analyses (Figs. 2 and 7). A similar behavior is observed for E_r, Fig. 9(b). In particular, the central (blue band) area is about 10 μm wide in agreement with the width estimated by SEM for the lens-shape dark structures in region C. Furthermore, mechanical results correlate well with the morphological images showing the most damaged zone of the strip (Fig. 4).

The presence of a softer area and with low reduced elastic modulus is compatible with the presence of abundant graphitic domains [34]. Battiato et al. have recently shown by nanoindentation experiments a reduction of the elastic properties in irradiated single-crystal diamond material [35]. Broitman et al. have also shown a correlation between the reduction in hardness and elastic modulus with the increase of sp^2 bonded material in diamond-like carbon films [36]). Our nano-indentation maps suggest that an effective and rather homogenous graphitization occurred throughout the whole region C, in agreement with spectroscopic results (Figs. 7 and 8). Here, the energy deposited by the laser beam is larger (center of the spot); moreover, overlapping phenomena between more consecutive laser scans are absent. On the other hand, the two larger areas on both sides of the central strip (corresponding to areas A and B) show a limited change in the mechanical properties, in agreement with the abundance of diamond phase, as proven by Raman experiments (Figs. 7 and 8) and confirmed by morphological changes (Fig. 3). As already discussed in Section 3.3, this feature can be justified considering that regions A and B receive a double irradiation dose, such that previously graphitized layers undergo ablation [7]. This process sequence allows interpreting the presence of the diamond peak (thin graphitic layer and inhomogeneous graphitization) and consequently a fluctuation of H and E_r values along the two regions.

Interestingly, at the boundary between A and B regions (bottom edge of Fig. 9(a) and (b)) a relatively soft region (colored in green and light blue) occurs. This behavior nicely correlates with the peculiar characteristic of the C zone, clearly identified by Raman analysis and described as a region with a relatively low diamond content.

3.5. Electrical measurements

In literature it is well known that graphitic contacts on diamond can work well as electrodes thanks to their good electric conduction property [12,13,16,37].

Current-voltage (I–V) measurements were carried out to evaluate the strip resistivity by means of the transmission line model method. First, a series of I–V tests were performed measuring at increased distance d between the two probes along the same graphite strip. Then, the total resistance R_T from each I–V curve was extracted. Plotting R_T

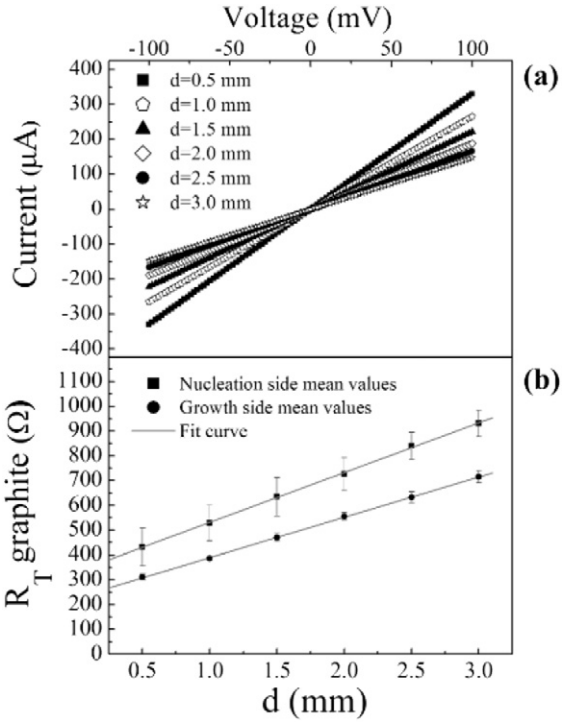

Fig. 10. (a) Typical I–V characteristics recorded on a graphite strip of the growth side varying the contact separation distance, *d*. (b) Mean values of the Resistance R_T plotted against the distance *d* between the probes for graphite electrodes produced on both nucleation (squares) and growth (dots) diamond surfaces.

as a function of the distance *d*, the probe contact resistance R_c and the resistivity ρ of the material under investigation are obtained by a linear fit of the experimental data according to:

$$R_T = 2R_C + \frac{\rho}{wt}d \tag{1}$$

where *w* and *t* are the width and the thickness of the strip, respectively.

Fig. 10 (a) shows typical I–V characteristics recorded on a graphite strip for a distance *d* varying from 0.5 mm to 3 mm (in steps of 0.5 mm). Each curve exhibits an almost linear trend, which confirms the ohmic nature of the graphitic strip and allows extrapolating a resistance value R_T for each separation by a linear fit. In order to allow for a more accurate estimate and for statistical analysis, this set of measurements was repeated on all the graphite contacts on each side. A good linearity of resistance as a function of probe separation was always found, confirming the reproducibility of the graphitization process. In particular, these measurements were performed first on the graphitic contacts produced on the polished diamond surface (nucleation side) and then on the unpolished diamond surface (growth side) with the aim of investigating if the diamond surface topography affects the result of the graphitization process.

Fig. 10(b) show the result obtained from the statistical analysis carried out on the experimental data for graphitic strips created on both nucleation and growth diamond sides. An estimate of the slopes was extracted from a linear fit providing mean values of (2.01 ± 0.03) × 10^5 Ω/m and (1.63 ± 0.02) × 10^5 Ω/m for the graphitic strips on the nucleation and growth side, respectively. Since the contact width is about 850 μm (measured by SEM) and assuming that the strip average thickness is about 180 nm (estimated value for a graphitic strip produced with similar irradiation conditions [18]), resistivity values of about (3.08 ± 0.14) × 10^{-5} Ωm and (2.50 ± 0.10) × 10^{-5} Ωm for nucleation and growth side respectively were obtained from the Eq. 1. These results are in good agreement with the expected one for graphite $\rho \approx 10^{-5} - 10^{-6}$ Ωm [7,13,18,28,38].

It is possible to observe that R_T data evaluated from the I–V curves recorded on the growth side graphitic strips are characterized by a lower standard deviation than those extracted from the measurements carried out on the nucleation side graphite strips. This result is ascribed to the probes/graphite electrode contacts, which result to be better and more reproducible thanks to the higher roughness of the back unpolished diamond side. This is also confirmed by the larger error bar in the plot of Fig. 10(b).

Subsequently, the electric insulation between strips was verified by contacting two coplanar graphitic strips. Exiguous currents of about some hundreds of fA were measured between strips produced on both diamond surfaces besides an almost linear behavior of the I–V curves over the investigated voltage range, from −10 V to +10 V, which suggests an ohmic nature for the graphite/diamond contact. Typical I–V characteristics recorded by contacting two coplanar graphitic strips for a distance d along the diamond surface are shown in Fig. 11(a). By using the TLM method we evaluated the diamond resistivity (Fig. 11(b)), which results to be of $(8.1 \pm 0.8) \times 10^9$ Ωm.

After these electrical investigations, it is possible to conclude that conductive graphitic contacts, with ohmic behavior, have been created on diamond surface taking advantage of diamond graphitization process induced by laser.

4. Conclusions

In this work, the manufacturing of large area graphitic contacts on diamond surface by laser-writing was carried out and critically analyzed. In particular, strip-like contacts were created on diamond surface of both sides, with orthogonal orientation, to obtain a segmented all-carbon device capable to give bi-dimensional information during detection processes for nuclear applications, such as the experiment PADME [20].

The characterization of the device by means of several different techniques allowed demonstrating that the effectiveness of a large-area graphitization can be tested by means of different, complementary experiments, which are sensitive to different properties of the modified material.

Scanning Electron Microscopy and micro-Raman Spectroscopy allowed understanding the physical evolution of the graphitization process, and in particular how the morphological and structural changes depend on laser processing. The two techniques indicate a strong periodicity of the surface modifications, correlated to the fabrication process. Then, phenomena of absorption from environment were found by EDS: oxidation reactions were present on all the irradiated areas, with increasing intensity values for the most damaged zones. Subsequently, hardness and elastic modulus mappings were performed showing that hard-soft transformation occurred depending on the locally deposited energy. The results correlate with the structural modification according to the change of hybridization ($sp^3 \rightarrow sp^2$) of carbon atoms, in agreement with SEM and micro-Raman results. Interestingly, both Raman and nano-indentation reveal a narrow C′ region, at the border between A and B areas, showing an intermediate graphitization degree, not recognized by SEM and EDS analyses. Nevertheless, some small morphological differences between A and B regions detected by SEM (Section 3.1) have not been validated by micro-Raman and mechanical investigations. It will be possible to examine further these details by subsequent more in-depth analysis.

Finally, current-voltage analyses allowed to verify the nature of the diamond-graphite contact and to evaluate the resistivity values of the strips. Good conductive properties and ohmic behavior were observed for all the graphitic strips, with a resistivity average around 2.5–3×10^{-5} Ωm along the strips. In addition, exiguous currents of about some hundreds of fA were measured between coplanar strips over the voltage range from −10 V to +10 V suggesting an ohmic nature for the graphite/diamond contact and making the strips suitable as electrodes in all-carbon sensors.

A final prototype of this all-carbon sensor was already tested by 550 MeV electron and positron beams at the BTF, Frascati (Italy) as an investigation preliminary to the PADME experiment. Data analysis is in progress and will be discussed in a following work.

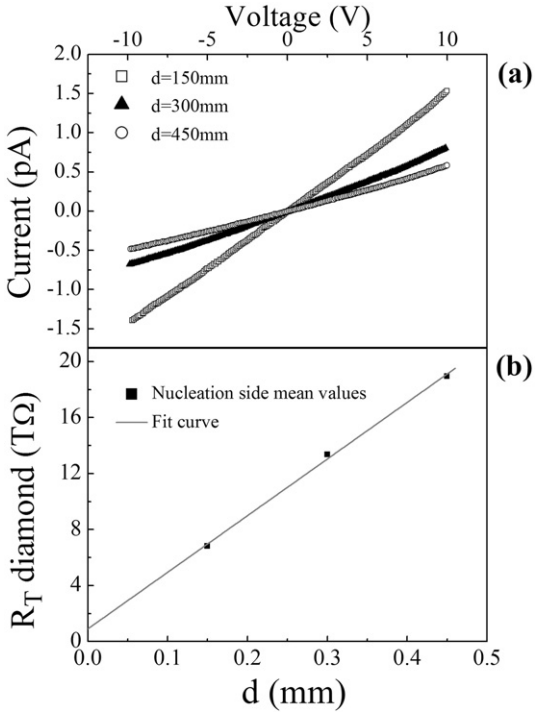

Fig. 11. (a) Typical I–V characteristics recorded on nucleation side by contacting two coplanar graphitic strips for a distance d. (b) Resistance R_T plotted against the distance d along the diamond surface.

Acknowledgments

The authors acknowledge Prof. A. Perrone (Department of Mathematics and Physics of Lecce) for valuable scientific discussions, and M. Corrado, G. Fiore, A. Miccoli, C. Pinto and M. Spedicato (INFN section of Lecce) for setting up the experimental apparatus and the instrumentations.

E. Broitman acknowledges financial support from the Swedish Government Strategic Research Area in Materials Science on Functional Materials at Linköping University (Faculty Grant SFO-Mat-LiU No 2009 00971).

References

[1] M. Rebai, C. Cazzaniga, G. Croci, M. Tardocchi, E. Perelli Cippo, P. Calvani, M. Girolami, D.M. Trucchi, G. Grosso, G. Gorini, Pixelated single-crystal diamond detector for fast neutron measurements, J. Instrum. 10 (2015), http://dx.doi.org/10.1088/1748-0221/10/03/C03016.

[2] J. Bol, S. Müller, E. Berdermann, W. de Boer, A. Furgeri, M. Pomorski, C. Sander, S. Udrea, D. Varenstov, Diamond thin film detectors for beam monitoring devices, Phys. Status Solidi A 204 (9) (2007), http://dx.doi.org/10.1002/pssa.200776328.

[3] A. Valentin, A. Tardieu, V. Mille, A. Tallaire, J. Achard, A. Gicquel, Polarization effect on time-of-flight measurements performed on a CVD diamond single crystal, Phys. Status Solidi A 212 (11) (2015) 1–5, http://dx.doi.org/10.1002/pssa.201532205.

[4] M. Bruzzi, C. De Angelis, M. Scaringella, C. Talamonti, D. Viscomi, M. Bucciolini, Zero-bias operation of polycrystalline chemically vapour deposited diamond films for intensity modulated radiation therapy, Diam. Relat. Mater. 20 (2) (2011) 84–92, http://dx.doi.org/10.1016/j.diamond.2010.11.011.

[5] S. Almaviva, M. Marinelli, E. Milani, A. Tucciarone, G. Verona-Rinati, R. Consorti, A. Petrucci, F. De Notaristefani, I. Ciancaglioni, Synthetic single crystal diamond diodes for radiotherapy dosimetry, Nucl. Inst. Methods Phys. Res. A 594 (2008) 273–277, http://dx.doi.org/10.1016/j.nima.2008.06.028.

[6] A. Galbiati, S. Lynn, K. Oliver, F. Schirru, T. Nowak, B. Marczewska, J.A. Dueas, R. Berjillos, I. Martel, L. Lavergne, Performance of monocrystalline diamond radiation

detectors fabricated using TiW, Cr/Au and a novel ohmic DLC/Pt/Au electrical con-tact, IEEE Trans. Nucl. Sci. 56 (2009) 1863–1874, http://dx.doi.org/10.1109/TNS. 2009.2020428.
[7] V.I. Konov, Laser in micro and nanoprocessing of diamond materials, Laser Photonics Rev. 6 (2012) 739–766.
[8] G. Conte, P. Allegrini, M. Pacilli, S. Salvatori, T. Kononenko, A. Bolshakov, V. Ralchenko, V. Konov, Three-dimensional graphite electrodes in CVD single crystal diamond detectors: charge collection dependence on impinging β-particles geome-try, Nucl. Inst. Methods Phys. Res. A 799 (2015) 10–16, http://dx.doi.org/10.1016/j. nima.2015.07.024.
[9] M. Girolami, L. Criante, F. Di Fonzo, S. Lo Turco, A. Mezzetti, A. Notargiacomo, M. Pea, A. Bellucci, P. Calvani, V. Valentini, D.M. Trucchi, Graphite distributed electrodes for diamond-based photon-enhanced thermionic emission solar cells, Carbon 111 (2017) 48–53.
[10] M. Shimizu, Y. Shimotsuma, M. Sakakura, T. Yuasa, H. Homma, Y. Minowa, K. Tanaka, K. Miura, K. Hirao, Periodic metallo-dielectric structure in diamond, Opt. Express 17 (1) (2009) 46.
[11] S. Su, J. Li, G.C.B. Lee, K. Sugden, D. Webb, H. Ye, Femtosecond laser-induced micro-structures on diamond for microfluidic sensing device applications, Appl. Phys. Lett. 102 (2013) 231913.
[12] S. Lagomarsino, M. Bellini, C. Corsi, F. Gorelli, G. Parrini, M. Santoro, S. Sciortino, Three-dimensional diamond detectors: charge collection efficiency of graphitic electrodes, Appl. Phys. Lett. 103 (2013) 233507.
[13] B. Sun, P.S. Salter, M.J. Booth, High conductivity micro-wires in diamond following arbitrary paths, Appl. Phys. Lett. 105 (2014) 231105.
[14] T.V. Kononenko, A.A. Khomich, V.I. Konov, Peculiarities of laser-induced material transformation inside diamond bulk, Diam. Relat. Mater. 37 (2013) 50.
[15] A. Oh, B. Caylar, M. Pomorski, T. Wengler, A novel detector with graphitic electrodes in CVD diamond, Diam. Relat. Mater. 38 (2013) 9.
[16] M. Pacilli, P. Allegrini, G. Conte, E. Spiriti, V.G. Ralchenko, M. Komlenok, A. Bolshakov, A.A. Khomich, V. Konov, Beta particles sensitivity of an all-carbon detector, Nucl. Inst. Methods Phys. Res. A 738 (2014) 119.
[17] J.C. Angus, Structure and thermochemistry of diamond, in: A. Paoletti, A. Tucciarone (Eds.), The Physics of Diamond, IOS Press, Oxford, UK 1997, pp. 9–30.
[18] M. De Feudis, A.P. Caricato, G. Chiodini, M. Martino, E. Alemanno, G. Maruccio, A.G. Monteduro, P.M. Ossi, R. Perrino, S. Spagnolo, Characterization of surface graphitic electrodes made by excimer laser on CVD diamond, Diam. Relat. Mater. 65 (2016) 137–143, http://dx.doi.org/10.1016/j.diamond.2016.03.003.
[19] M. De Feudis, A.P. Caricato, G. Chiodini, M. Martino, G. Maruccio, A.G. Monteduro, P.M. Ossi, R. Perrino, S. Spagnolo, Diamond detectors with electrodes graphitized by means of laser, Proceeding of the Conference Incontri di Fisica delle Alte Energie IFAE, 39 C, Il Nuovo Cimento, Italy, Rome 2016, p. 254, http://dx.doi.org/10.1393/ncc/i2016-16254-5.
[20] M. Raggi, V. Kozhuharov, Proposal to search for a dark photon in positron on target collisions at DAΦNE Linac, Adv. High Energy Phys. 2014 (2014), ID 959802. http://dx.doi.org/10.1155/2014/959802.
[21] R. Essig, J. A. Jaros, W. Wester, P. H. Adrian, S. Andreas, T. Averett, O. Baker and B. Batell et al., Dark Sectors and New, Light, Weakly-coupled Particles, arXiv: 1311.0029 [hep-ph]
[22] C. Patrignani, et al., Review of Particle Physics, Chin. Phys. C 40 (100001) (2016) (Particle Data Group).
[23] Aepplied Diamond Inc. (USA), http://usaplieddiamond.com/
[24] W. Oliver, G. Pharr, Measurement of hardness and elastic modulus by instrumented indentation: advances in understanding and refinements to methodology, J. Mater. Res. 19 (1) (2004) 3–20.
[25] G.K. Reeves, H.B. Harrison, Obtaining the specific contact resistance from transmis-sion line model measurements, IEEE Electron Device Lett. 3 (1982) 111–113, http://dx.doi.org/10.1109/EDL.1982.25502.
[26] H. Ohfuji, T. Okuchi, S. Odake, H. Kagi, H. Sumiya, T. Irifune, Micro−/nanostructural investigation of laser-cut surfaces of single- and polycrystalline diamonds, Diam. Relat. Mater. 19 (2010) 1040.
[27] M. Huang, F. Zhao, Y. Cheng, N. Xu, Z. Xu, Mechanisms of ultrafast laser-induced deep-subwavelength gratings on graphite and diamond, Phys. Rev. B 79 (2009) 125436.
[28] S. Lagomarsino, M. Bellini, C. Corsi, S. Fanetti, F. Gorelli, I. Liontos, G. Parrini, M. Santoro, S. Sciortino, Electrical and Raman-imaging characterization of laser-made electrodes for 3D diamond detectors, Diam. Relat. Mater. 43 (2014) 23.
[29] A.C. Ferrari, D.M. Basko, Nat. Nanotechnol. 8 (2013) 235–246.
[30] I. Pócsik, M. Hundhausen, M. Kóos, L. Ley, J. Non-Cryst. Solids 227–230 (1998) 1083–1086.
[31] C. Castiglioni, F. Negri, M. Rigolio, G. Zerbi, J. Chem. Phys. 115 (2001) 3769–3778.
[32] C. Castiglioni, M. Tommasini, G. Zerbi, Philos. Trans. R. Soc. Lond. Ser. A - Math. Phys. Eng. Sci. 362 (2004) 2425–2459.
[33] R.R. Nair, P. Blake, A.N. Grigorenko, K.S. Novoselov, T.J. Booth, T. Stauber, N.M.R. Peres, A.K. Geim, Fine structure constant defines visual transparency of graphene, Science 320 (2008) 1308.
[34] A. Richter, R. Ries, R. Smith, M. Henkel, B. Wolf, Nanoindentation of diamond, graph-ite and fullerene films, Diam. Relat. Mater. 9 (2000) 170–184.
[35] A. Battiato, M. Lorusso, E. Bernardi, F. Picollo, F. Bosia, D. Ugues, A. Zelferino, A. Damin, J. Baima, N.M. Pugno, E.P. Ambrosio, P. Olivero, Softening the ultra-stiff: controlled variation of young modulus in single-crystal diamond, Acta Mater. 116 (2016) 95–103.
[36] E. Broitman, N. Hellgren, Z. Czigany, R.D. Twesten, J. Luning, I. Petrov, L. Hultman, B.C. Holloway, Structural and mechanical properties of diamond-like carbon films deposited by direct current magnetron sputtering, J. Vac. Sci. Technol. A 21 (4) (2003) 851–859.
[37] M.P. Ray, J.W. Baldwin, T.I. Feygelson, J.E. Butler, B.B. Pate, Note: laser ablation tech-nique for electrically contacting a buried implant layer in single crystal diamond, Rev. Sci. Instrum. 82 (2011) 056105.
[38] G. Parrini, F. Fabbrizzi, S. Lagomarsino, L. Nunziati, S. Sciortino, A. Scorzoni, Laser graphitization for polarization of diamond sensors, Proceedings of Science, 10th In-ternational Conference on Large Scale Applications and Radiation Hardness of Semi-conductor Detectors, 2011 (Italy, Firenze).